Journal of The Electrochemical Society, 2022 **169** 064505

Durability Testing of Low-Iridium PEM Water Electrolysis Membrane Electrode Assemblies

Maximilian Möckl,[1,2,z] Matthias F. Ernst,[3] Matthias Kornherr,[3] Frank Allebrod,[4] Maximilian Bernt,[2,3,a] Jan Byrknes,[5] Christian Eickes,[5] Christian Gebauer,[6] Antonina Moskovtseva,[4] and Hubert A. Gasteiger[3]

[1]*Technical University of Munich, School of Engineering and Design, Department of Energy and Process Engineering, Institute for Electrical Energy Storage Technology, 80333 Munich, Germany*
[2]*ZAE Bayern, Electrochemical Energy Storage, 85748 Garching, Germany*
[3]*Technical University of Munich, Department of Chemistry, Chair of Technical Electrochemistry, 85748 Garching, Germany*
[4]*H-TEC Systems GmbH, 86167 Augsburg, Germany*
[5]*Greenerity GmbH, Industriegebiet Süd E11, 63755 Alzenau, Germany*
[6]*Heraeus Deutschland GmbH & Co. KG, 63450 Hanau, Germany*

Lowering the iridium loading at the anode of proton exchange membrane (PEM) water electrolyzers is crucial for the envisaged GW-scale deployment of PEM water electrolysis. Here, the durability of a novel iridium catalyst with a low iridium packing density, allowing for low iridium loadings without decreasing the electrode thickness, is being investigated in a 10-cell PEM water electrolyzer short stack. The anodes of the membrane electrode assemblies (MEAs) of the first five cells utilize a conventional iridium catalyst, at loadings that serve as benchmark for today's industry standard (2 $mg_{Ir}\,cm^{-2}$). The last five cells utilize the novel catalyst at 8-fold lower loadings (0.25 $mg_{Ir}\,cm^{-2}$). The MEAs are based on Nafion® 117 and are tested for 3700 h by load cycling between 0.2 and 2.0 $A\,cm^{-2}$, with weekly polarization curves and impedance diagnostics. For both catalysts, the performance degradation at low current densities is dominated by an increase of the overpotential for the oxygen evolution reaction (OER), whereby the OER mass activity of the novel catalyst remains ≈4-fold higher after 3700 h. The temporal evolution of the OER mass activities of the two catalysts will be analyzed in order to assess the suitability of the novel catalyst for industrial application.

 [DOI: 10.1149/1945-7111/ac6d14]

Manuscript submitted February 17, 2022; revised manuscript received April 19, 2022. Published June 8, 2022. *This paper is part of the JES Focus Issue on Advanced Electrolysis for Renewable Energy Storage.*

A large-scale production of hydrogen by water electrolysis offers the possibility to store large amounts of electrical energy from fluctuating renewable sources. The chemically stored energy can then be transported and used flexibly in terms of time and space. Thus, an extensive defossilization of different sectors (mobility, industry, heat) could be achieved and possible supply gaps could be bridged more easily and cost-efficiently than with electrical storage alone.[1–3]

Several water electrolysis technologies exist: The three most important are alkaline electrolysis (AEL), PEM (proton exchange membrane) water electrolysis (PEMWE), and solid oxide electrolysis (SOE). The AEL is a long established technology that has been implemented on the MW scale, with demonstrated electrolyzer lifetimes of ca. 100,000 h.[4] Similar lifetimes have been achieved for PEMWE, which is already available on an industrial scale as well, but needs further development, especially with regard to mass production.[4] On the other hand, the SOE technology is not yet commercialized on the MW scale and its lifetime is at least one order of magnitude lower compared to AEL and PEMWE,[4] so that the latter two will likely be the most prominent technologies in the near future. However, PEMWE has several advantages: Hydrogen can be produced at elevated pressure (30 to 40 bar) with a highly dynamic power range directly from purified water, whereby the H_2 quality remains high even at higher pressures, and only few and simple purification steps are necessary to reach high purity.[5] In addition, the current density at rated full-power is at ≈2 $A\,cm^{-2}$ for commercial PEMWEs and thus about four-fold higher than that of AELs (≈0.5 $A\,cm^{-2}$), a difference which will very likely increase further in the future[4].

In order to achieve a significant impact of renewable hydrogen, very large production capacities have to be installed in the coming decades. Bernt et al.[6] estimated the necessary electrolysis power installation for a full defossilization of the mobility sector (i.e., a complete replacement of fossil transportation fuels) until the end of the 21st century to be in the range of ≈150 GW/year. Although most of the materials for the PEMWE are available in sufficient quantities even for such large scale-up rates, the resource constraints of the platinum group metals that are required for the PEMWE catalysts are very critical. At the cathode, typically platinum on a carbon support (at current loadings of ≈0.5–1.0 $mg_{Pt}\,cm^{-2}$) is used to catalyze the hydrogen evolution reaction (HER), whereas at the anode iridium based catalysts (at current loadings of ≈2 $mg_{Ir}\,cm^{-2}$) are used for the oxygen evolution reaction (OER).[7] However, the currently high platinum loadings at the cathode are less of a concern, as they can be reduced by an order of magnitude without any performance losses, due to the fast kinetics of the HER in the acidic PEMWE environment.[6,8–10] In contrast, the OER kinetics at the anode are very slow, so that any lowering of the iridium catalyst loading leads to decreasing efficiencies at the same current density, in the best case amounting to an additional kinetic overpotential at the anode of ≈50 mV for a 10-fold reduction in iridium loading.[6,11,12] In practice, with current iridium catalysts, the anode loadings cannot be reduced to below ≈0.5 $mg_{Ir}\,cm^{-2}$, as this results in anode catalyst layers that are too thin to achieve a homogenous electrical contacting of the electrode. Lower loadings would require catalysts with a much reduced iridium packing density (in terms of $g_{Ir}\,cm^{-3}$ electrode);[6,11] these are difficult to achieve, since there are no electrically conductive support materials that are stable at the high anodic potentials of the PEMWE anode. Since there is currently no equally stable and active alternative for iridium as anode catalyst for a PEMWE,[8,13,14] a strong increase in PEMWE deployment could lead to a shortage of iridium. According to a platinum group metal (PGM) market report,[15] the iridium demand in 2018 was ≈6.8 t, reasonably consistent with the estimated iridium supply of ≈8.4 t in

[a]Present address: Freudenberg FST GmbH, Bayerwaldstr. 3, 81737 München, Germany.
[z]E-mail: maximilian.moeckl@zae-bayern.de

2018 (based on the South African production of ≈6.8 t and the South African share of the world-wide iridium production of ≈81%.[16]) For an electrolyzer efficiency of 70% referenced to the lower heating value (LHV; corresponding to a cell voltage of 1.79 V), current commercial PEMWEs yield a current density of ≈1.5 A cm^{-2} and have an anode catalyst loading of ≈2 mg_{Ir} cm^{-2}, resulting in an iridium-specific power density of ≈0.75 g_{Ir}/kW. Thus, with the currently installed PEMWE technology, only ≈10 GW of newly installed PEMWE power per year would already require ≈7.5 t of iridium per year, which would essentially consume the entire world-wide iridium supply, and thus would not allow for the large-scale deployment of PEMWEs at the above mentioned rate required to defossilize the transport sector.

To overcome this obstacle, recent studies suggest the need for a substantial reduction of the anode iridium loading to at least 0.25–0.4 mg_{Ir} cm^{-2},[8,17] or, more precisely, to loadings that are low enough to reach iridium-specific power densities of ≈0.01 g_{Ir}/kW at 70%$_{LHV}$ that are estimated to be necessary for a large-scale PEMWE deployment.[6] One option to reduce the iridium-specific power density at a given iridium loading is to reduce the non-kinetic performance losses of a PEMWE, so that higher current densities and thus higher power densities could be obtained at the same cell voltage and efficiency. By far the largest share of non-kinetic losses is currently caused by ohmic resistances due to proton conduction across the relatively thick membranes (≈180 μm for Nafion® 117).[18] If thinner membranes are used, a substantial fraction of these losses can be eliminated. Laboratory experiments with thinner membranes (conducted with conventional catalysts loadings and at 80 °C) reached current densities at an efficiency of 70%$_{LHV}$ ranging from ≈3.3 A cm^{-2} (90 μm Aquivion® C98-09S)[19]) to 4.0 A cm^{-2} (50 μm Nafion® 212[20]) all the way up to ≈4.8 A cm^{-2} (30 μm Nafion® XL[21]); this may be compared to ≈1.7 A cm^{-2} for a ≈180 μm thick Nafion® 117 membrane under the same conditions.[12,18] Thus, reducing membrane thickness can result in an up to ≈3-fold increase in current density at the same cell voltage/efficiency, corresponding to a ≈3-fold increase in power density. However, when using thin membranes, the increasing product gas crossover must be taken into account. From a safety perspective, the hydrogen crossover from the cathode to the anode side is particularly important. The use of thin membranes can severely limit the minimum current density where the system can be operated safely without countermeasures.[18,22,23] Possible mitigation strategies for excessive hydrogen crossover include the incorporation of chemical recombination catalysts into the membrane electrode assembly (MEA),[24–27] or the integration of recombination catalysts either at some point in the O_2 outlet stream at the anode side of the electrolyzer or at the back side of the anode porous transport layer (PTL).[28]

Based on the above discussion, simply using thinner membranes can increase the power density by ≈3-fold, so that with a conventional iridium loading of 2 mg_{Ir} cm^{-2}, iridium-specific power densities of ≈0.25 g_{Ir}/kW at 70%$_{LHV}$ should be reachable. As a matter of fact, this was demonstrated for an MEA based on a 50 μm Nafion® 212 membrane with an anode iridium loading of ≈1.6 mg_{Ir} cm^{-2} and a cathode platinum loading of ≈0.30 mg_{Pt} cm^{-2}, operated at 80 °C and ambient pressure.[6] A further lowering of the iridium-specific power density, however, requires a reduction of the anode iridium loading. As shown in references[6] and,[29] current commercial OER catalysts that are based on a thick, electrically conductive IrO_2 coating applied on a non-conductive TiO_2 support (for example Umicore Elyst Ir75 0480, further on referred to as 'Benchmark catalyst') are limited by the insufficient in-plane electrical conductivity and the inhomogeneity of the thin electrode layers that result at low iridium loadings of approximately <0.5 mg_{Ir} cm^{-2}. This could be remedied by an electrically conductive support material on which the active iridium particles are finely dispersed, in analogy to the carbon supported platinum catalysts (Pt/C) that are used at the cathode (e.g., the thickness of an only ≈0.03 mg_{Pt} cm^{-2} cathode electrode based on a ≈5wt% Pt/C catalyst is ≈11 μm.[6]) Possible candidates are antimony-doped tin oxide (ATO),[30,31] niobium-doped titanium oxide (NTO),[32,33] or tungsten doped titanium oxide.[34] Nevertheless, the long-term stability of these support materials in the acidic environment of a PEMWE is still under investigation. Another approach toward low loadings is the use of iridium thin-films which can be coated directly on highly structured membranes[35] or on nano structures (e.g., whiskers) on the membrane surface.[36]

Within the framework of the Kopernikus P2X project,[37] the partners Greenerity GmbH, Heraeus Deutschland GmbH & Co. KG and Technical University of Munich (TUM) investigated a catalyst concept that would allow for low iridium loadings without decreasing the electrode thickness, i.e. a concept that would offer a reduced iridium packing density in the electrode. It is based on utilizing a non-conductive TiO_2 support material coated with a thin layer of an amorphous, hydrous iridium oxide (a-IrO$(OH)_x$), as shown by Tovini et al. for the Benchmark catalyst,[38] but utilizing a low specific surface area TiO_2 support.[39] With this approach, a substantial reduction of the iridium packing density from ≈2.3 g_{Ir} cm^{-3} for the Benchmark catalyst to ≈0.5 g_{Ir} cm^{-3} for the newly designed catalyst is possible (further on referred to as "P2X" catalyst),[39] which now enables the preparation of sufficiently thick electrodes of, e.g., ≈5 μm at iridium loadings of 0.25 mg_{Ir} cm^{-2} (with the Benchmark catalyst, this loading would result in an electrode thickness of only ≈1 μm, too thin for a well-performing electrode[6]). In addition to enabling thicker electrodes at low iridium loadings, this new P2X catalyst was shown to enable a ≈8-fold reduction in iridium loading at even a ≈50 mV better begin-of-life (BOL) performance compared to the Benchmark catalyst.[39] Part of this better performance can be attributed to the higher intrinsic activity for the oxygen evolution reaction (OER) of the a-IrO$(OH)_x$ coating of the P2X catalyst compared to the more crystalline and thus less OER active IrO_2 of the Benchmark catalyst.[40,41] However, a platinum-coated PTL is required for the P2X catalyst, owing to the lower intrinsic conductivity of a-IrO$(OH)_x$ compared to crystalline IrO_2.[39,42] In combination with a 50 μm thick Nafion® 212 membrane, the performance of MEAs with the P2X catalyst at a loading of 0.27 mg_{Ir} cm^{-2} is projected to yield a current density of ≈4 A cm^{-2} at 1.79 V (i.e., at an efficiency of 70%$_{LHV}$) when operated at 80 °C and ambient pressure,[39] which would correspond to an iridium-specific power density of ≈0.04 g_{Ir}/kW, within a factor of 4 of the above stated long-term target (in comparison, the projected value for the Benchmark catalyst under the same conditions is ≈0.4 g_{Ir}/kW[39]).

Apart from the initial performance of a new catalyst, however, its long-term stability is another important factor for its use in actual applications. PEMWE systems should have a long service life, so that the at the moment still high investment costs of 1000 to 1400 $/kW (with near-future projected costs for large scale production of ≈400 $/kW[43]) are as low as possible when translated into operating time, whereby commercial PEMWEs already have a lifetime of ≈100,000 h.[4] However, testing a new catalyst over such a long period is difficult to implement in practice, especially in the early stages of catalyst development. Yet, as will be shown, even shorter operating times of several thousand hours can provide a robust initial indication of catalyst durability, which is done most efficiently in a short stack configuration. Therefore, 5 MEAs each with the Benchmark and the P2X catalyst were tested at 60 °C and ambient pressure in a 10-cell PEMWE short stack with an active area of 30 cm^2 over a period of 3700 h, cycling the current density between 0.2, 1.0, and 2.0 A cm^{-2}. Every week, full polarization curves were recorded, together with acquiring the high frequency resistance (HFR) of each cell. This allowed to determine the cell voltage degradation rate as well as the iR-free cell voltage degradation rate as a function of current density. Furthermore, a Tafel analysis of the iR-free cell voltages at low current densities allowed for a quantification of the OER mass activity vs. time for the two different catalysts, providing further insights into the relative stability of the new P2X catalyst compared to the commercial Benchmark catalyst. Finally, the observed evolution of the HFR over time will be discussed.

Experimental

Membrane electrode assemblies (MEAs) and test stack.— 30 cm^2 active area MEAs based on Nafion® 117 membranes were prepared by Greenerity GmbH according to the specifications of the used stack type ELS-30 with 10 cells from H-TEC Systems GmbH. A commercial carbon-supported platinum catalyst was used for the cathode electrodes with a loading of 0.3 $mg_{Pt}\,cm^{-2}$ for the HER. Two different catalysts were used on the anode side as described by Bernt et al.[39] : i) a commercial Benchmark catalyst consisting of mostly crystalline IrO_2 deposited as thick film on a high surface area TiO_2 support (75wt% iridium; Elyst Ir75 0480 from Umicore, Germany); ii) the newly developed P2X catalyst based on hydrous iridium oxide deposited as thin film on a lower surface area TiO_2 support (49.2wt% iridium from Heraeus, Germany; note that the wt % iridium for this catalyst batch is slightly higher than that reported in reference[39]). The Benchmark catalyst was applied at a loading of 2.0 $mg_{Ir}\,cm^{-2}$, resulting in an anode electrode thickness of ≈7.4 μm, while the P2X catalyst was applied at a loading of 0.25 $mg_{Ir}\,cm^{-2}$, resulting in an anode electrode thickness of ≈3.5 μm. The MEAs were assembled in a 10-cell short stack by H-TEC Systems in two groups. The first five cells contained the MEAs with the Benchmark catalyst and the last five cells the MEAs with the P2X catalyst. Platinized titanium PTLs were used on the anode side to prevent progressive passivation of the titanium in contact with the electrode and to ensure a low contact resistance.[39,44] All 11 individual bipolar/monopolar plate potentials are accessible from the outside by fine pins, which allow monitoring of the individual cell voltages and of individual impedance spectra. The stack has a water inlet and water/O_2 outlet at the anode side and a single H_2/water outlet at the cathode side. Thus, water feed and flow field purging is possible at the anode side of the stack only. Although the outflowing water at the cathode side could in principle be tested for dissolved iridium species by ICP-MS as shown, e.g. by Knoeppel et al.,[45] the measurements however would be biased by the contact of the water to non-noble metal surfaces in the stack which would lead to galvanic redeposition of iridium species.[45]

Short stack test station and operation.— A fully automated test station from Horiba-Fuelcon was used for conducting the short stack test. It is equipped with an impedance meter (True-Data-EIS from Sensotech, Germany) in combination with a multiplexer. This allows sequential impedance measurements to be made at any DC current within the range of the electrical power source on all 10 cells in the stack without changing the connections during the test. Furthermore, all individual cell potentials were recorded simultaneously during the whole test.

The temperature of the stack was controlled via the anode water circuit, whereby the water temperature at the inlet of the stack was kept at 60 °C. Higher operating temperatures around 80 °C would in principle be beneficial for an accelerated stress test, but the temperature in this study was limited to 60 °C based on the recommendation by the stack manufacturer. In order to achieve a relatively uniform temperature distribution in the stack and to avoid excessive in-plane temperature differences across the flow fields (with a maximum temperature difference between inlet and outlet of ≈5 K at 2.0 $A\,cm^{-2}$), the water flow rate was set to 3.3 ml/(min cm^2).[21] To ensure continuously high water quality, only highly purified make-up water was used (water processed by ULTRA CLEAR® TP ultrapure water system from Evoqua, USA). Additionally, a two stage cleanup system was installed in the anode water recirculation loop, comprising a larger deionization vessel (5 L resin volume) behind the main feed water pump and a second smaller cartridge (250 ml resin volume) close to the stack, both filled with mixed bed resin (Leycopure from Leyco, Germany). The second cartridge and all further tubing and fittings on the remaining water path to the stack were made from plastics (SAN, PP or PTFE) to prevent metal ion leaching into the feed water, and thus possible ionic contamination of the MEAs.[46,47]

X-ray photoelectron spectroscopy.— To investigate the near-surface chemical state and composition of the P2X and the Benchmark catalyst, X-ray photoelectron spectroscopy (XPS) was performed using an Axis Supra System (Kratos, UK). XPS spectra were recorded with a monochromatic Al Kα source (1486.6 eV) at a pass energy of 40 eV, using a step size of 0.05 eV and a dwell time of 1000 ms. XPS samples were prepared by finely dispersing the catalyst powders in a mixture of 2-propanol (purity ⩾ 99.8%, from Sigma Aldrich, Germany) and ultrapure water (Milli-Q® IQ 7005 water purification system from Merck, Germany), and then drop-casting the resulting ink on a non-conductive Gylon® substrate (type 3545, from Garlock, USA). Infrared radiation was used to evaporate the solvent. Before insertion into the ultra-high vacuum chamber for analysis, the samples were dried at 50 °C under vacuum overnight. The samples were analyzed without sputter cleaning, and the C 1s line of adventitious carbon at 284.6 eV was used to correct the binding energies of all recorded spectra. Data treatment was carried out using the program CasaXPS with application of a Shirley background.

MEA cross sections and scanning electron microscopy.— Cross Sections from a pristine Benchmark and P2X MEA sample as well as a Benchmark and a P2X MEA harvested after the durability test from the short stack were investigated via scanning electron microscopy (SEM). For this, small snippets cut from the active area of the MEAs were sandwiched between copper tape and polished with a cryo cross Section polisher (IB-19520CCP from JEOL, Japan) at −80 °C and at an acceleration voltage of 6 kV, followed by a fine-mode step at 4 kV. Afterwards, the cross Sections were examined with a scanning electron microscope (JSM-IT200 from JEOL, Japan) in order to evaluate the membrane thicknesses at BOL and EOT.

Electrochemical measurement procedures and test sequences.— The stack test was started by a warm-up phase of several hours without applying a current and with water circulation only in order to reach a steady water inlet temperature of 60 °C and to heat up the stack. The water inlet temperature was kept constant, and cathode and anode side were kept at ambient pressure during the whole durability test. After a subsequent conditioning for 20 min at 0.1 $A\,cm^{-2}$, the first galvanostatically controlled BOL polarization curves for all 10 cells of the short stack were recorded, stepwise changing the current from 33 mA cm^{-2} to 2.2 $A\,cm^{-2}$ (11 steps) and allowing for an equilibration time of 10 min at each current density. At 0.2, 1.0, and 2.0 $A\,cm^{-2}$, galvanostatically controlled AC impedance spectra for each cell were recorded at 15 frequencies, ranging from 15 kHz to 150 mHz. The perturbation current amplitude was 0.5 A (≡0.017 $A\,cm^{-2}$) at 0.2 $A\,cm^{-2}$, and 5.0 A (≡0.17 $A\,cm^{-2}$) at 1.0 $A\,cm^{-2}$ and 2.0 $A\,cm^{-2}$ in order to maintain a linear system response at a reasonable signal to noise ratio. The high frequency resistance (HFR) for each cell in the stack was obtained at a fixed frequency of 6.9 kHz, which consistently represents the first measuring point after the real axis intercept in the Nyquist plot.

After BOL characterization, the stack was subjected to a durability protocol that consisted of repeatedly cycling the current density between three levels for 10 minutes each, namely 0.1, 1.75, and 2.0 $A\,cm^{-2}$. This protocol emulates an intermittent operation without any shut-down phases, i.e., avoiding periods at open-circuit-voltage (OCV) in order to prevent catalyst dissolution by repeated reduction/oxidation events.[48] After each 7 day period of continuous current cycling (i.e., after every 168 h or after every set of 336 current cycles), another set of polarization curves and impedance spectra was recorded according to the above mentioned scheme. This procedure was continued over ≈3700 h.

At several points during the ≈3700 h durability test, certain events that are not part of the above durability test sequence (system maintenance, external errors by auxiliary equipment, etc.; see Table I) forced a short shut-down of the test station. The first

Table I. List of events that required a temporary shut-down of the test station during the ≈3700 h durability test. The right-hand column shows the time during the durability test at which a given event occurred.

Event type	Occurence (h)
exhaust line blocked	350
water supply system maintenance	1180, 2380, 3220
critical software updates	1270, 1370, 2040, 3530
maintenance of security relevant system components	3050

polarization curve directly after such an event was always recorded, but was not used in the regression analysis of the degradation rate and of the OER mass activity evolution, due to the observed transient performance increase after each of the shut-down and start-up cycles. This is caused by a change in the catalyst surface properties of the iridium of the OER catalyst (reduction to hydrous iridium oxide during the OCV period upon shut-down, and re-oxidation to iridium oxide after start-up), which was shown to temporarily affect its OER activity.[48] However, all of these thus biased performance data are depicted as red symbols in the presented performance/OER mass activity versus time plots (Figs. 3, 4, 6 and 7).

Results and Discussion

XPS based estimation of the relative iridium utilization of the catalysts.—X-ray photoelectron spectroscopy (XPS) measurements were carried out to estimate the ratio of the active (hydrous) iridium oxide film thickness on the TiO_2 support between the P2X and the Benchmark catalyst.

Considering that only the outermost surface of the (hydrous) iridium oxide film is catalytically active for the OER, and assuming a (hydrous) iridium oxide film thickness (t_{film}) of more than a few monolayers, the ratio of t_{film} of the Benchmark catalyst over that of the P2X catalyst ($t_{film\ (Benchmark)}/t_{film\ (P2X)}$) would correspond to the ratio of the iridium utilization (u_{Ir}) of the P2X catalyst over that of the Benchmark catalyst ($u_{Ir\ (P2X)}/u_{Ir\ (Benchmark)}$). On the basis of the known iridium content of the catalysts, of the specific surface areas of the TiO_2 supports (estimated to be $\approx 100\ m^2\ g^{-1}$ for the Benchmark catalyst and $\approx 50\ m^2\ g^{-1}$ for the P2X catalyst), and assuming the deposition of a homogeneous (hydrous) iridium oxide film, Bernt et al. estimated that $t_{film\ (Benchmark)}/t_{film\ (P2X)} \approx 6$ nm/2 nm $\approx$ 3.0/1,[39] which in turn suggests that the iridium utilization of the P2X catalyst should be ≈3-fold higher for the P2X catalyst (i.e., $u_{Ir\ (P2X)}/u_{Ir\ (Benchmark)} \approx$ 3.0/1). In this case, if the surface-normalized, so-called specific OER activity of the two catalysts were to be the same, the P2X catalyst would be expected to have a ≈3-fold higher mass activity for the oxygen evolution reaction (OER). However, since the specific OER activity of hydrous iridium oxide (as is the case for the P2X catalyst) is ≈10-fold higher than that of iridium oxide (as is the case for the Benchmark catalyst),[40,41] the beginning-of-life OER mass activity of the P2X catalyst should be ≈30-fold higher than that of the Benchmark catalyst, which is in reasonably good agreement with the experimentally observed ≈37-fold higher OER mass activity.[39]

Alternatively to the approach taken by Bernt et al.,[39] the relative thickness of the (hydrous) iridium oxide films between the Benchmark and the P2X catalyst can also be estimated by the following XPS analysis of the Ir $4p_{3/2}$ and the Ti 2p intensities (here taken as the sum of Ti $2p_{1/2}$ and Ti $2p_{3/2}$) of the (hydrous) iridium oxide film and the TiO_2 support, respectively. Qualitatively, it is obvious already from the XPS data shown in Fig. 1, that the ratio of the Ir $4p_{3/2}$ over the Ti 2p intensities (i.e., of the areas under the two spectral features) is much smaller for the P2X compared to the Benchmark catalyst, indicating a substantially thinner (hydrous) iridium oxide film thickness.

In order to quantify this observed difference, the following considerations and approximations are taken: (i) both XPS features

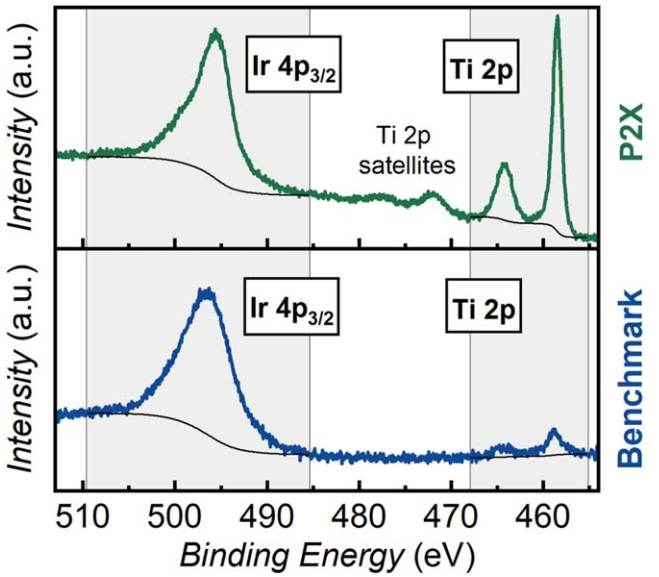

Figure 1. X-ray photoelectron spectra of the P2X (green line) and of the Benchmark (blue line) catalyst samples. Ir $4p_{3/2}$ signals of the (hydrous) iridium oxide films and Ti 2p signals of the TiO_2 supports are recorded with a step size of 0.05 eV. The thin black line represents the Shirley background that was subtracted to obtain the peak areas given in Table II.

occur in a rather narrow binding energy range (≈455–505 eV), so that the kinetic energy of the photoelectrons is also very similar (≈982–1032 eV); (ii) for such a narrow kinetic energy range, the inelastic mean free path (λ) of the Ir $4p_{3/2}$ and the Ti 2p photoelectrons is essentially identical (≈3.0 nm based on Shea and Dench;[49]) (iii) for essentially identical λ values, the instrumental sensitivity factor ratio of the Ir $4p_{3/2}$ and the Ti 2p features corresponds to the ratio of their Scofield cross-sections; (iv) the radius of the TiO_2 particles is at least 2-fold larger than λ (for the estimated $100\ m^2\ g^{-1}$ BET TiO_2 support of the Benchmark catalyst, $r_{TiO_2} \approx 7$ nm;[39]) and, v) the (hydrous) iridium oxide film homogeneously covers the TiO_2 support. For a hypothetical planar geometry, the (hydrous) iridium oxide film thickness (t_{film}) on the TiO_2 support could then be calculated based on the following equation (equation (1) in reference,[50] corrected, however, for the wrong sign in the original publication):

$$t_{film} = \lambda \cdot cos(\theta) \cdot ln\left(1 + \frac{(I_{Ir\ 4p_{3/2}})/(s_{Ir\ 4p_{3/2}})}{(I_{Ti\ 2p})/(s_{Ti\ 2p})}\right) \quad [1]$$

Here, $I_{Ir4p_{3/2}}$ and $I_{Ti\ 2p}$ are the experimentally measured peak intensities for a given catalyst, $s_{Ir\ 4p_{3/2}}$ and $s_{Ti\ 2p}$ are the Scofield cross-sections,[51] and θ is the angle between the surface normal of a planar sample and the photoelectron analyzer (for a planar sample, $\theta = 0°$ in the XPS system used here). For the non-planar samples used here, θ is not anymore constant, but assuming that the size and the morphology of the Benchmark and the P2X catalyst are similar, the spatial variation of θ should also be similar, so that the ratio of

t_{film} of the Benchmark catalyst over that of the P2X catalyst can be estimated as:

$$t_{\text{film (Benchmark)}}/t_{\text{film (P2X)}} \approx \frac{ln\left(1+\frac{(I_{\text{Ir }4p_{3/2}})/(s_{\text{Ir }4p_{3/2}})}{(I_{\text{Ti }2p})/(s_{\text{Ti }2p})}\right)_{\text{Benchmark}}}{ln\left(1+\frac{(I_{\text{Ir }4p_{3/2}})/(s_{\text{Ir }4p_{3/2}})}{(I_{\text{Ti }2p})/(s_{\text{Ti }2p})}\right)_{\text{P2X}}} \quad [2]$$

Based on the data tabulated in Table II, this yields a (hydrous) iridium film thickness ratio of $t_{\text{film (Benchmark)}}/t_{\text{film (P2X)}} \approx 2.1/1$. This is clearly smaller than the film thickness ratio of ≈3 that was estimated by Bernt et al.[39] by assuming that the BET surface area of the TiO_2 support of the Benchmark catalyst would be ≈100 $m^2\,g^{-1}$. While the latter assumption is reasonable, the actual TiO_2 BET cannot be determined, but if the true value were ≈67 $m^2\,g^{-1}$, the iridium utilization ratio obtained via the BET-based estimate and via our XPS analysis would be identical. Owing to the uncertainty in the TiO_2 BET estimate, we consider the XPS-based iridium utilization ratio of ≈2.1 to be the more reliable value.

MEA performance and long-term performance degradation.— For a first overview of the performance of the new P2X anode catalyst compared to the Benchmark anode catalyst over the course of the long-term performance test, Fig. 2 shows a comparison of the averaged polarization curves for both MEA types at beginning-of-life (BOL; squares), after 890 h (circles) as well as at the end-of-test (EOT) after 3700 h (triangles). Figures 2a and b show the polarization curves and the HFR values at 60 °C and ambient pressure, averaged over the five MEAs with the Benchmark anode catalyst at a loading of 2.0 $mg_{Ir}\,cm^{-2}$ (error bars represent the standard deviation), while Figs. 2c and d show the analogous data for the P2X catalyst at a loading of 0.25 $mg_{Ir}\,cm^{-2}$. The solid lines in Figs. 2a and c represent the measured cell voltages (E_{cell}) and the dashed lines the iR-free cell voltage ($E_{iR\text{-free}}$), corresponding to E_{cell} corrected by the HFR ($E_{iR\text{-free}} = E_{cell} - i \cdot HFR$). The HFR values were obtained from the electrical impedance spectra recorded at three current densities (0.2, 1.0, and 2.0 A cm^{-2}) and were used for the iR-correction of several current densities, as marked by the gray shaded areas in Fig. 2.

A first inspection of the data in Figs. 2a and c reveals the good reproducibility of the cell voltage performance of each set of five MEAs, expressed by the small error bars: The maximum variation occurs at the highest current density of 2.2 A cm^{-2}, with less than ±22 mV at BOL and less than ±16 mV at EOT. A closer look at the BOL polarization curves (squares) reveals a ≈20 mV lower cell voltage (solid lines) and iR-free cell voltage (dashed lines) of the P2X catalyst MEAs compared to the Benchmark catalyst MEAs over the whole current density range, with the HFR values of both MEA types being identical (≈185 mΩ cm^2). Thus, the higher initial performance of the P2X catalyst at an 8-fold lower iridium loading, as reported by Bernt et al.[11] for 5 cm^2 active area single-cell measurements, can also be observed for the measurements in a 30 cm^2 active area 10-cell short stack shown here. Calculating the iridium-specific power density at a cell voltage efficiency of 70%$_{LHV}$ (≡1.79 V), the P2X catalyst MEAs reach a value of 0.11 g_{Ir}/kW, which is ≈10-fold lower than the 1.0 g_{Ir}/kW obtained for the Benchmark MEAs.

Looking at the temporal evolution of the iR-free cell voltage (dashed lines in Figs. 2a and c), which allows for a closer inspection of the evolution of the anode catalyst activity, two aspects stand out: first, for both catalyst types, the iR-free cell voltage performance and thus the catalyst activity decreases (visible by the up-shift of the iR-free polarization curves) and second, this performance decay is clearly most pronounced during the first 890 h (circles) compared to the following 2810 h until EOT. Over the first 890 h, the Benchmark catalyst MEAs show an average $E_{iR\text{-free}}$ increase at 1 A cm^{-2} of ≈50 mV, whereas the average $E_{iR\text{-free}}$ of the P2X catalyst MEAs is slightly higher, amounting to ≈70 mV. In contrast, for the following 2810 h there is no change visible for the Benchmark catalyst MEAs and a less than ≈15 mV increase for the P2X catalyst MEAs. In fact, the iR-free EOT performance of both MEA types is approximately the same, with the iR-free cell voltage of the P2X catalyst MEAs at 2.2 A cm^{-2} being only ≈12 mV higher than that of the Benchmark catalyst MEAs, even though the former have an 8-fold lower iridium loading.

When again considering the non-corrected cell voltages (solid lines in Figs. 2a and c), a further effect becomes apparent for both MEA types. The slope of the E_{cell} vs. current density curves at current densities greater than 0.5 A cm^{-2} clearly decreases with time, which is caused by a decreasing HFR, as shown in Figs. 2b and d. The overall HFR decrease over the 3700 h of testing is ≈25% on average, but slightly more pronounced for the Benchmark catalyst MEAs (from 186 to 134 mΩ cm^2) than for the P2X catalyst MEAs (from 184 to 145 mΩ cm^2). This leads to the phenomenon that at high current densities, the HFR drop for the Benchmark MEAs is strong enough to overcompensate the catalyst activity decay, resulting in a slightly higher current density of 1.18 A cm^{-2} at EOT at the 70%$_{LHV}$ efficiency benchmark (i.e., at 1.79 V) compared to BOL, whereas the current density of the P2X catalyst MEAs at the same voltage decreases slightly to 1.04 A cm^{-2} at EOT. When evaluating the iridium-specific power densities at 70%$_{LHV}$ for the two MEA types at EOT, there still remains a ≈7-fold advantage of the P2X compared to the Benchmark catalyst MEAs (0.13 g_{Ir}/kW for the former and 0.95 g_{Ir}/kW, respectively). At the highest current density of 2.2 A cm^{-2}, also the P2X catalyst MEAs show slightly higher EOT performance compared to BOL, due to the HFR decrease outweighing the catalyst activity decay.

To better quantify the above observations and to gain more insights into the MEA performance degradation mechanisms, we will next discuss the degradation rates at different current densities. Due to the weekly recording of polarization curves and impedance spectra, a closer look at the MEA performance degradation is possible. Figure 3 shows the temporal evolution of the mean cell voltages (E_{cell}) for both the Benchmark catalyst MEAs (Figs. 3a) and the P2X catalyst MEAs (Fig. 3b) at three current densities, corresponding to the low, mid, and high power density regime (0.2 A cm^{-2} (squares), 1.0 A cm^{-2} (circles), and 2.0 A cm^{-2} (triangles)). As mentioned before, all red marked symbols represent biased polarization curves due to preceding shut-down events (listed in Table I). Looking at the evolution of E_{cell} over time reveals two clearly distinguishable time-dependent phenomena at 0.2 and 1.0 A cm^{-2}: in the time period from BOL up to ≈1000 h, the cell voltage shows an initially rather fast increase that gradually levels off, whereas in the subsequent time period, from ≈1000 h onwards,

Table II. Summary of the analysis of the Ti 2p (sum of Ti $2p_{1/2}$ + Ti $2p_{3/2}$) and of the Ir $4p_{3/2}$ XPS features obtained for the P2X and the Benchmark catalyst. The Shirley background corrected areal intensities ($I_{Ti\ 2p}$ and $I_{Ir4p_{3/2}}$) are determined from Fig. 1 and the Scofield cross-sections ($s_{Ti\ 2p}$ and $s_{Ir\ 4p_{3/2}}$) are taken from reference 51.

Catalyst	XPS features	Areal Intensity I	Scofield cross-section s
P2X	Ti $2p_{1/2}$ + Ti $2p_{3/2}$	2776	7.91
	Ir $4p_{3/2}$	5747	5.59
Benchmark	Ti $2p_{1/2}$ + Ti $2p_{3/2}$	616	7.91
	Ir $4p_{3/2}$	7592	5.59

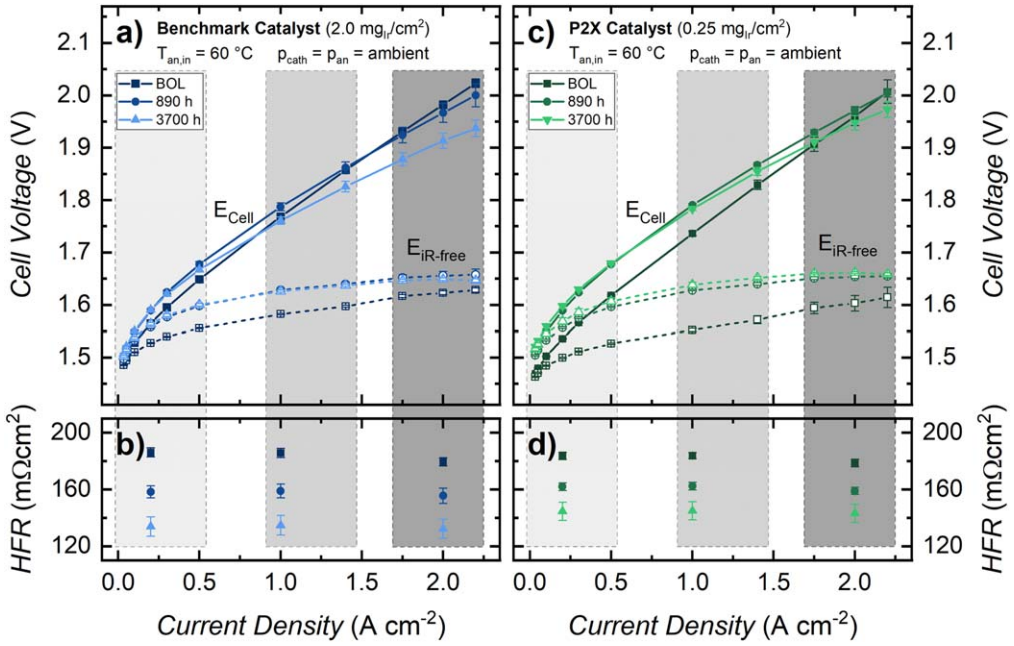

Figure 2. Averaged polarization curves of 30 cm^2 active area Nafion® 117 based MEAs (from 5 MEAs each, with error bars representing the standard deviation) at BOL (squares) as well as after 890 h (circles) and 3700 h (triangles) of the load cycling durability test (switched every 10 min between 0.1, 1.75, and 2.0 A cm^{-2}), recorded with a 10-cell short stack at ambient pressure and 60 °C anode water inlet temperature (3.3 ml$_{H2O}$/(min cm^2)): (a) of the MEAs with the Benchmark anode catalyst at a loading of 2.0 mg$_{Ir}$ cm^{-2}; (c) of the MEAs with the P2X anode catalyst at a loading of 0.25 mg$_{Ir}$ cm^{-2}. The same Pt/C based cathode catalyst is used for both MEA types at a loading of 0.3 mg$_{Pt}$ cm^{-2}. The solid lines show the measured cell voltages (E_{cell}), while the dashed lines represent the iR-free cell voltage corrected by the HFR ($E_{iR\text{-}free}$). b) & d) Averaged HFR values and standard deviation for the two sets of MEAs, determined from impedance measurements for all cells at three different current densities (0.2, 1.0, and 2.0 A cm^{-2}). The iR-correction is done by using the same HFR value for several current densities, as marked by the gray shaded areas in the figure.

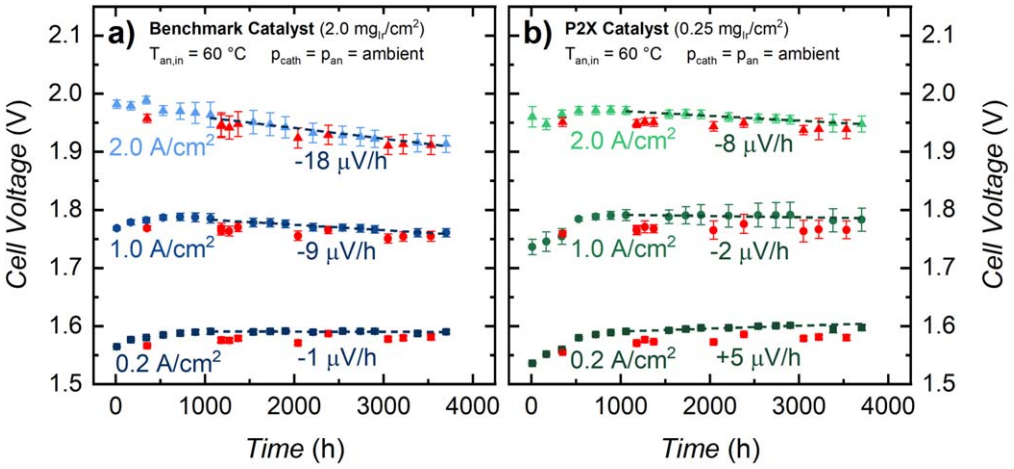

Figure 3. Temporal evolution of the mean cell voltage during prolonged load cycling (switched every 10 min between 0.1, 1.75, and 2.0 A cm^{-2}) of a 10-cell short stack at 60 °C anode water inlet temperature and ambient pressure: a) average and standard deviation of E_{cell} of the five Benchmark catalyst MEAs (2.0 mg$_{Ir}$ cm^{-2}); b) average and standard deviation of E_{cell} of the five P2X catalyst MEAs (0.25 mg$_{Ir}$ cm^{-2}). The E_{cell} values are taken from weekly performed polarization curves at the current densities of 0.2 A cm^{-2} (squares), 1.0 A cm^{-2} (circles), and 2.0 A cm^{-2} (triangles). The average cell voltage degradation rates are evaluated between 1000 h and 3700 h for each current density by means of a linear regression fit (dashed black lines). All red marked symbols show values from polarization curves which were recorded directly after a shut-down event of the test station, and thus are excluded from the regression analysis (a complete list of shut-down events is given in Table I).

the evolution of E_{cell} with time is rather linear. The increase of E_{cell} during the first ≈1000 h is more prominent for the P2X catalyst than for the Benchmark catalyst, consistent with the results shown in Figs. 2a and c (i.e., comparing the performance at BOL and after 890 h). From ≈1000 h onwards, the cell voltages remain almost constant at the low current density of 0.2 A cm^{-2} (reflected in low rates of voltage change of −1 and +5 μV/h for the Benchmark and the P2X catalyst MEAs, respectively), and even show a clearly decreasing trend at the high current density of 2.0 A cm^{-2} (with −18 and −8 μV/h for the Benchmark and the P2X catalyst MEAs, respectively), which can be attributed to the decrease of the HFR with time (see 2b and (d)) that positively affects the cell voltage. Overall, the degradation rates evaluated between 1000 and 3700 h are consistently lower (or more negative) for the Benchmark catalyst MEAs compared to the P2X catalyst MEAs.

Comparing our data with long-term test results from other groups reveals a similar behavior, with a stabilization of the cell voltage at around 1000 h, following an initial phase with higher degradation

rates. Siracusano et al.[52] report an initial degradation rate of ≈90 μV/h during a 1000 h steady-state test at a rather high current density of 3.0 A cm^{-2}, which attenuated to 33 μV/h during the last 300 h, and they attribute this rather slow stabilization to mass transfer resistances or to a change of the oxidation state of the anode catalyst surface. However, their MEAs feature an IrRuOx catalyst at the anode side and are based on thinner, 90 μm Aquivion® membranes, which renders a quantitative comparison with our data in Fig. 3 difficult. Also Danilovic et al.[53] show averaged cell voltage data for a long-term electrolysis test (60,000 h) of two different industrial stack design evolution levels, whereby the cell voltage change rates are highest during the first 1000 h. However, there are also results in the literature where such an initial increase or nonlinear change is not immediately visible. In a publication by Rakousky et al.,[44] the cell voltage evolution is shown during galvanostatic operation at 2.0 A cm^{-2} for 400 h, using a platinized anode PTL. The cell voltage remains at a stable level while the HFR shows a gradual decrease of the ohmic cell resistance by ≈10%, which the authors attribute to a reduced contact resistance between the PTLs and the electrodes, caused by a gradual membrane creep into the pores of the PTLs. Since the change in ohmic resistances (e.g., contact resistances and membrane resistances) over the course of a durability test can mask the effect of catalyst degradation on the cell voltage evolution, a better understanding on the long-term stability of different catalysts can be obtained by analyzing the iR-free cell voltage evolution.

Using the cell voltages and the HFR values from the regularly performed polarization curves and impedance measurements, a closer look at the electrode aging can be taken by evaluating the temporal evolution of the iR-free cell voltage. Figures 4a and b thus show the mean iR-free cell voltage for the Benchmark and the P2X catalyst MEAs, respectively, determined at three current densities (0.2, 1.0, and 2.0 A cm^{-2}). Again, measurement points that were recorded directly after shut-down events of the test station are marked in red and are not used for the analysis. For both MEA types, the electrode aging is most pronounced during the first 1000 h. The average performance decay in this initial time period at the three different current densities ranges between ≈30-50 mV for the Benchmark catalyst MEAs, while it is somewhat larger for the P2X catalyst MEAs (≈60-80 mV). Interestingly, however, the iR-free cell voltages at the three different current densities are essentially identical after 1000 h, which is due to the initially ≈25-30 mV superior performance of the P2X catalyst MEAs (despite its 8-fold lower iridium loading), owing to the substantially higher intrinsic OER activity of the P2X catalyst compared to the Benchmark catalyst.

Following the stabilization of the iR-free cell voltages after the first 1000 h, both MEA types show only single-digit μV/h changes of the iR-free voltage, when determined by a linear regression analysis between 1000 h and the EOT at 3700 h. At 0.2 A cm^{-2}, the mean iR-free cell voltage of the Benchmark catalyst MEAs is increasing at a rate of +1 μV/h, whereas that of the P2X catalyst MEAs shows a clearly higher increase of +6 μV/h, pointing toward a faster decay of the OER activity of the P2X catalyst compared to the Benchmark catalyst. At the higher current densities of 1.0 and 2.0 A cm^{-2}, the degradation rates should in principle be equal or higher (i.e., more positive), since any possible mass transport related resistances in the electrodes would be expected to become more prominent at higher current densities. Surprisingly, however, the μV/h changes of the iR-free cell voltage at 2.0 A cm^{-2} are lower, namely -1 μV/h for the Benchmark catalyst MEAs (i.e., 2 μV/h lower than at 0.2 A cm^{-2}) and +1 μV/h for the P2X catalyst MEAs (i.e., 5 μV/h lower than at 0.2 A cm^{-2}). This, we believe, must be due to small errors in the quantification of the absolute values of the HFR, as is illustrated by the following analysis: Assuming that the degradation rates of the iR-free cell voltage of the P2X catalyst MEAs at 2.0 A cm^{-2} were to be at least the same as that at 0.2 A cm^{-2} (i.e., +6 μV/h), its iR-free cell voltage at 2.0 A cm^{-2} and 3700 h would have to be at least ≈14 mV higher (from Δ 5 μV/h ·2700 h ≈ Δ 14 mV), which would be obtained if the HFR measured at 3700 h were to be ≈7 mΩ cm^2 higher (from 7 mΩ cm^2 ·2.0 A cm^{-2} ≈ 14 mV), which amounts to a difference of only ≈5% of the measured HFR between 870-3700 h (≈160-145 mΩ cm^2, see Fig. 2(c)). As this corresponds to the expected accuracy of our HFR measurements, one must conclude that the iR-free cell voltage change rates at 2.0 A cm^{-2} cannot be determined reliably to better than approximately ±5 μV/h. On the other hand, for the analysis of current densities of 0.2 A cm^{-2} or below, the absolute error in determining the iR-free cell voltage is an order of magnitude lower and, in addition, it can be assumed that any mass transport effects are also negligible at such low current densities, so that an analysis at 0.2 A cm^{-2} or below should allow for a rather accurate quantification of any changes of the OER catalyst activity over time. Therefore, we will next examine the OER mass activity evolution of the two types of anode catalyst by conducting a Tafel analysis in the low current density region.

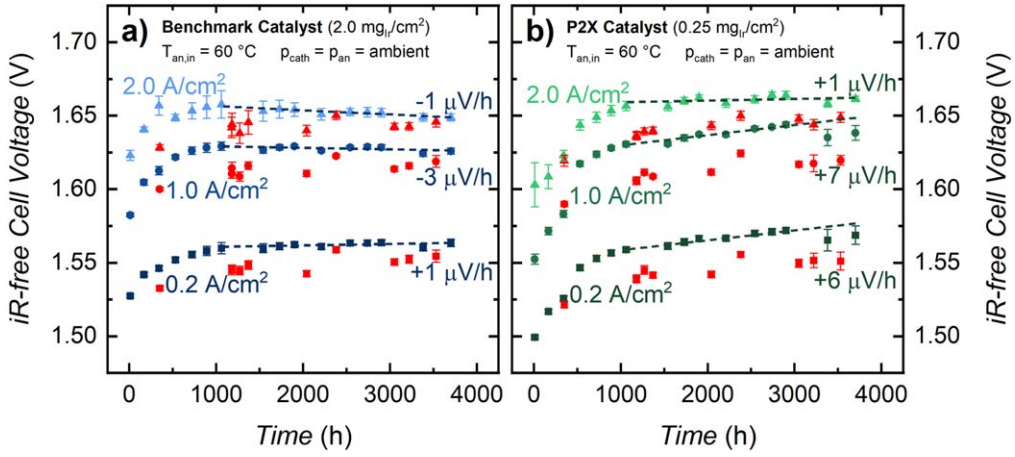

Figure 4. Temporal evolution of the mean iR-free cell voltage during prolonged load cycling (switched every 10 min between 0.1, 1.75, and 2.0 A cm^{-2}) of a 10-cell short stack at 60 °C anode water inlet temperature and ambient pressure: (a) average and standard deviation of $E_{iR\text{-}free}$ of the five benchmark catalyst MEAs (2.0 mg$_{Ir}$ cm^{-2}); (b) average and standard deviation of $E_{iR\text{-}free}$ of the five P2X catalyst MEAs (0.25 mg$_{Ir}$ cm^{-2}). The $E_{iR\text{-}free}$ values are taken from weekly performed polarization curves and impedance measurements at the current densities of 0.2 A cm^{-2} (squares), 1.0 A cm^{-2} (circles), and 2.0 A cm^{-2} (triangles). The average iR-free cell voltage degradation rates are evaluated between 1000 h and 3700 h for each current density by means of a linear regression fit (dashed black lines). All red marked symbols show values from polarization curves which were recorded directly after a shut-down event of the test station, and thus are excluded from the regression analysis (a complete list of shut-down events is given in Table I).

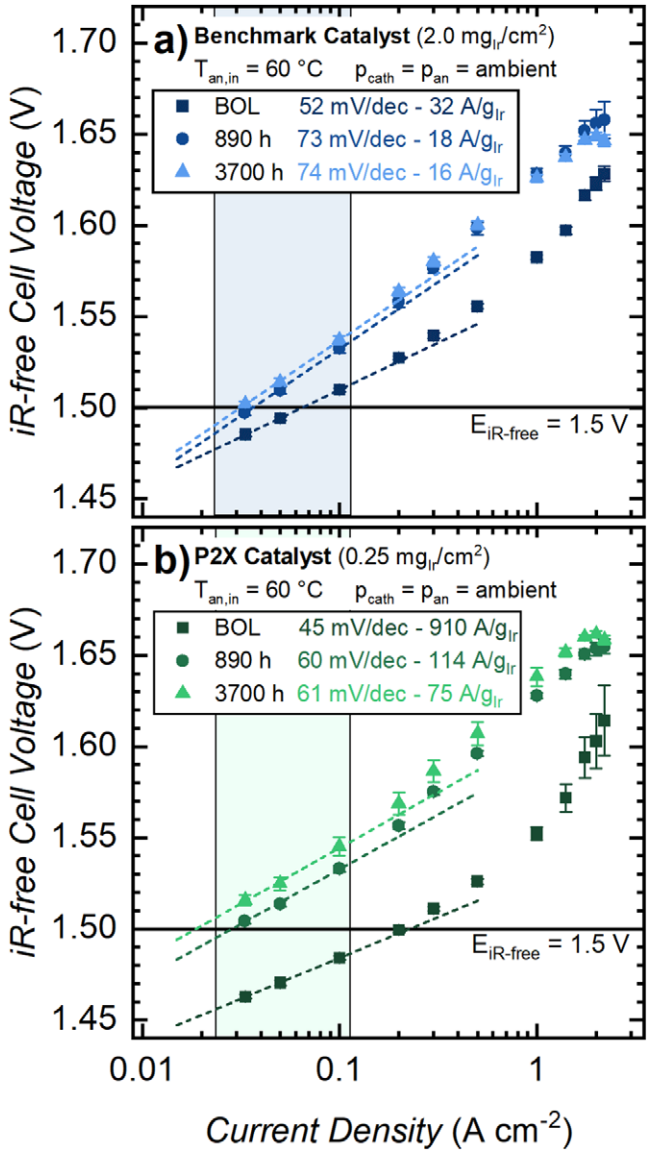

Figure 5. Tafel plot of the iR-free cell voltage vs. the logarithm of the current density for the two different MEA types at BOL (squares) as well as after 890 h (circles) and 3700 h (triangles) of the load cycling durability test, recorded at ambient pressure and 60 °C anode side water inlet temperature (same data as the dashed lines in Figs. 2a and c): (a) of the Benchmark anode catalyst (at 2.0 $mg_{Ir}\,cm^{-2}$); b) of the P2X anode catalyst (at 0.25 $mg_{Ir}\,cm^{-2}$). A linear regression fit between 33 and 100 mA cm^{-2} is used to obtain the Tafel slopes (dashed lines). Additionally, the OER mass activities of the catalysts at $E_{iR\text{-}free} = 1.5$ V are determined by the value of the respective fitted Tafel line at $E_{iR\text{-}free} = 1.5$ V. OER mass activity values at $E_{iR\text{-}free} = 1.5$ V and Tafel slopes are given in the legend inside the figure.

OER mass activity evolution of the benchmark and the P2X catalyst.—To gain better insight into the change of the OER kinetics of both catalysts, Figs. 5a and b show the averaged Tafel plots (i.e., $E_{iR\text{-}free}$ vs. the logarithm of the current density) at ambient pressure and at 60 °C anode water inlet temperature of the five Benchmark and the five P2X catalyst MEAs, respectively, recorded at BOL (squares) as well as after 890 h (circles) and 3700 h (triangles) of the durability test (same data as shown by the dashed lines in Figs. 2a and c). A linear regression fit of the data between 33 and 100 mA cm^{-2} is used to obtain the Tafel slopes (dashed lines in Fig. 5). Considering the negligible overpotential for the hydrogen evolution reaction (HER) at the here used cathode loadings of 0.3 $mg_{Pt}\,cm^{-2}$ ($\eta_{HER} \ll 5$ mV at 1 A cm^{-2}[26]) and the expected negligible mass transport resistances at low current densities, the fitted Tafel lines should very closely represent the OER activity of the two catalysts. Consequently, the OER mass activities of the catalysts at an iR-free cell voltage of 1.5 V are determined from current density values of the fitted Tafel lines at $E_{iR\text{-}free} = 1.5$ V, normalized by the anode catalyst loading.

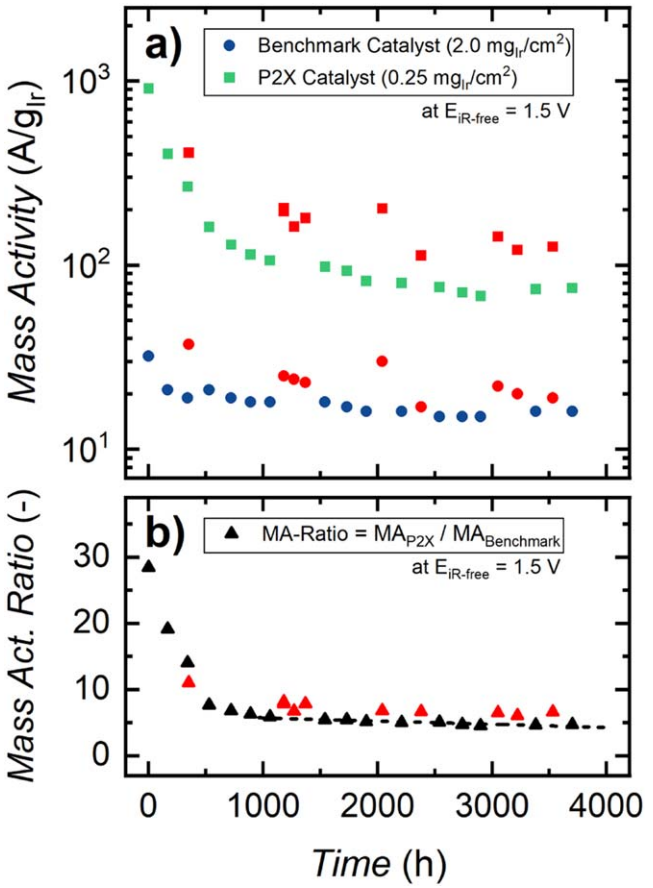

Figure 6. a) Temporal evolution of mean OER mass activity at 1.5 V iR-free cell voltage (ambient pressure, 60 °C anode water inlet temperature) for the Benchmark catalyst MEAs (circles, 2.0 $mg_{Ir}\,cm^{-2}$) and for the P2X catalyst MEAs (squares, 0.25 $mg_{Ir}\,cm^{-2}$). b) Temporal evolution of the OER mass activity ratio between the P2X catalyst and the Benchmark catalyst MEAs. All red marked symbols show values from polarization curves, which were recorded directly after a shut-down event of the test station (for a complete list of shut-down events see Table I).

In line with the results presented in the previous figures, two major findings stand out: At first, the P2X catalyst exhibits a ≈30-fold higher initial mass activity at $E_{iR\text{-}free} = 1.5$ V of 910 A/g_{Ir} compared to 32 A/g_{Ir} for the Benchmark catalyst (see legends in Figs. 5a and b). This is due to the fact that the former consists mostly of the more OER active hydrous iridium oxide, while the latter consists of less OER active iridium oxide[39] (note that the pristine Benchmark catalyst was shown to consist of a ≈50/50 mixture of crystalline and amorphous IrO_2.[38]) The higher OER mass activity of the P2X catalyst is also reflected in its rather low initial Tafel slope of 45 mV/dec (see legends in Figs. 5a and b) that is typical for hydrous iridium oxide based OER catalysts[39]; while the higher Tafel slope of 52 mV/dec obtained for the Benchmark catalyst is typical for iridium oxide based OER catalysts.[6,48] Second, both catalysts show a decline in OER mass activity and an increase in Tafel slope over the course of the prolonged cycling test. The OER mass activity decline is clearly more pronounced for the P2X catalyst than for the Benchmark catalyst, with the P2X catalyst's OER mass activity decreasing by a factor of ≈12 to 75 A/g_{Ir} after 3700 h, in contrast to only a factor of ≈2 in case of the Benchmark catalyst, namely to

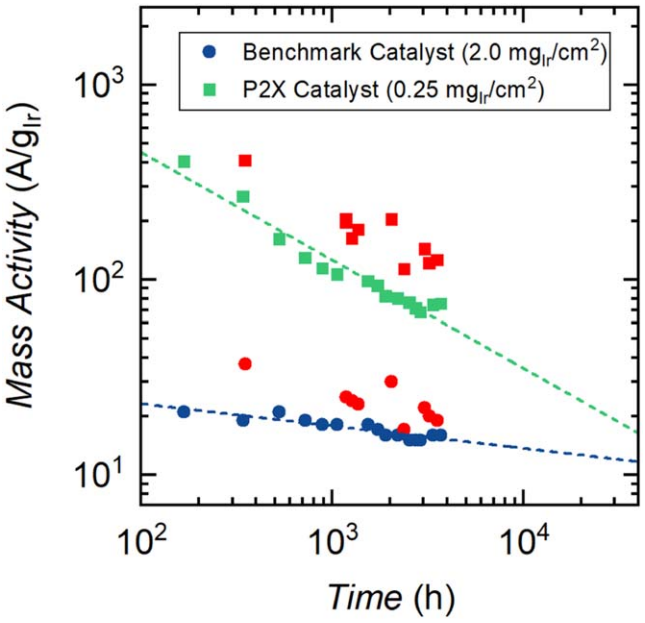

Figure 7. Double logarithmic plot of the mean OER mass activities at 1.5 V iR-free cell voltage (recorded at ambient pressure, 60 °C anode water inlet temperature; same data as in Fig. 6) for the Benchmark catalyst MEAs (blue circles, 2.0 $mg_{Ir}\,cm^{-2}$) and for the P2X catalyst MEAs (green squares, 0.25 $mg_{Ir}\,cm^{-2}$). The dashed lines are linear regression fits of the logarithm of the OER mass activities ($i_m^{*(1.5V)}$, in units of A/g_{Ir}) versus the logarithm of time (t, in units of h): $\log(i_m^{*(1.5V)}) = (-0.114 \pm 0.015)\cdot\log(t) + (1.593 \pm 0.046)$ for the Benchmark catalyst MEAs and $\log(i_m^{*(1.5V)}) = (-0.553 \pm 0.037)\cdot\log(t) + (3.760 \pm 0.117)$ for the P2X catalyst MEAs (excluding the data taken directly after a shut-down, marked in red).

16 A/g_{Ir} after 3700 h. At the same time, the Tafel slope of the P2X catalyst increases from 45 to 61 mV/dec, suggesting a gradual transformation of the hydrous iridium oxide into iridium oxide[39]. An increase in Tafel slope is also observed for the Benchmark catalyst, namely from 52 to 72 mV/dec, which may be indicative of the gradual transformation of the initially partially amorphous iridium oxide into predominantly crystalline iridium oxide over extended times at high anodic potentials.[54,55]

In order to obtain a better resolution of the time evolution of the OER mass activities, the weekly recorded polarization curves were also subjected to the same type of Tafel analysis. The results are shown in Fig. 6, whereby the red marked symbols represent the measurements that directly followed a system shut-down event (as mentioned above, the OER activity of the anode catalysts increases after system shut-downs during which the anode got exposed to crossover hydrogen, an effect that had been discussed previously[48]). Figure 6a shows the temporal evolution of the OER mass activity for the P2X catalyst (squares) and the Benchmark catalyst (circles), while Fig. 6b shows the evolution of the ratio of the OER mass activities of the P2X catalyst over that of the Benchmark catalyst.

As expected based on the literature,[40,41] the P2X catalyst based on hydrous iridium oxide is significantly more active at BOL than the Benchmark catalyst (≈30-fold, as shown in Fig. 6b) that is based on a mixture of amorphous and crystalline iridium oxide[38]. The temporal evolution of the OER mass activity reflects the above observed relatively fast rise in cell voltage and iR-free cell voltage over the first 1000 h (see Figs. 3 and 4, respectively), with both catalysts showing a relatively fast initial drop in the OER mass activity over the first 1000 h (see Fig. 6a), whereby the OER activity of the P2X catalyst drops much more rapidly, so that its OER mass activity benefit over the Benchmark catalyst shrinks to ≈6-fold after 1000 h (see Fig. 6b). This initially fast decay, however, is followed by a rather slow decrease over the remaining 2700 h until EOT, at which point the OER mass activity benefit of the P2X catalyst seems to stabilize at a factor of ≈4. Considering that the OER activity is highest for hydrous iridium oxide and lowest for crystalline iridium oxide,[40] we believe that the rather fast OER mass activity decay of the P2X catalyst in the first 1000 h observed here is due to a gradual conversion of the hydrous iridium oxide phase at the high anode potential during electrolysis to an amorphous iridium oxide phase, which over longer times becomes more crystalline.[54,55] On the other hand, the Benchmark catalyst that starts out with a roughly 50/50 mixture of amorphous and crystalline iridium oxide,[38] experiences a much slower OER activity decay, presumably due to an intrinsically slower conversion of amorphous to crystalline iridium oxide. Over much longer times than the 3700 h examined here, we would thus expect that the intrinsic OER activities of the two catalysts should become identical, which in terms of OER mass activity would imply that the P2X catalyst should retain a long-term OER mass activity benefit over the Benchmark catalyst by a factor that corresponds to the iridium utilization ratio, namely ≈2.1 (see Section 3.1).

Zero-order estimate of the longer-term catalyst-specific degradation rates.—While it would be desirable to test the performance of the P2X anode catalyst and to compare it to the performance of the Benchmark catalyst over much longer times, this is unfortunately not practical. However, in the following we will attempt to project the decay of the catalytic activity of the two catalysts on the basis of the OER mass activity data shown in Fig. 6. As described above, the OER mass activity at a low iR-free cell voltage (here 1.5 V) is a good quantitative descriptor for catalyst performance, since it is determined at very low current densities (i.e., between 33-100 mA cm^{-2}, see Fig. 5), where other voltage losses (e.g., due to mass transport resistances) and correction errors (e.g., due to imperfect HFR correction) have only minimal influence. Therefore, we need to emphasize that the thus projected voltage losses are only those that can be ascribed to OER mass activity losses and that possible additional voltage losses due to other aging mechanisms are not included (e.g., buildup of interfacial contact resistances, changes in mass transport resistances, membrane/ionomer degradation, etc.).

In order to project the catalyst mass activity losses over time, its functional dependence on time would have to be known. As the latter is not directly evident in Fig. 6, we have replotted the OER mass activity data from Fig. 6 in terms of the logarithm of the mass activity versus the logarithm of time in Fig. 7. Here, the data at BOL (nominally after 1 hour) are excluded, because the stack had been preconditioned at the manufacturer's site over the course of several tens of hours at different operating conditions, so that the mass activity values directly at the start of our experiment (BOL) do not represent the initial state of the catalyst. For the mass activities obtained from the second polarization curve after ≈200 h (first point shown in Fig. 7) and for any later measurements, however, this uncertainty in time is negligible. Surprisingly, the logarithm of the mass activity versus the logarithm of time follows a perfectly linear relationship for both catalysts between ≈200–3700 h, marked by the dashed linear regression lines in Fig. 7 (note that the red data points that represent data taken directly after a shut-down event were excluded from the fit). While the fundamental mechanistic reason for this empirically observed relationship is unclear, it does hold over about 1.3 decades in time, so that it should serve as a reasonable zero-order estimate for projecting the drop in mass activity over another decade of time, i.e., from the end-of-test at ≈3700 h to ≈40,000 h. The measured values for the OER mass activity at an iR-free cell voltage of 1.5 V after 3700 h ($i_{m\,(3700\,h)}^{*(1.5V)}$) are 15.3 A/$g_{Ir}$ for the Benchmark catalyst and 61 A/g_{Ir} for the P2X catalyst, whereas the extrapolated values for $i_{m\,(40,000\,h)}^{*(1.5V)}$ are 11.7 ± 0.4 A/g_{Ir} for the Benchmark catalyst and 16.4 ± 1.5 A/g_{Ir} for the P2X catalyst (marked by the dashed lines in Fig. 7; the fitting Eqs. are given in the Fig. caption; the uncertainties of the extrapolated mass activities are calculated by using the standard errors of the slopes of the fits which are ±0.015 for the Benchmark catalyst and ±0.037 for the P2X

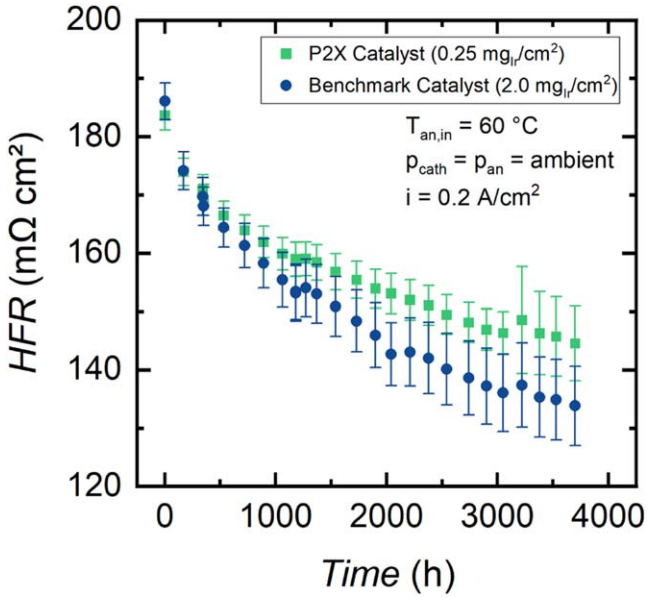

Figure 8. Temporal evolution of the HFR acquired at 0.2 A cm^{-2} and averaged for each type of MEA, namely for the five Benchmark catalyst MEAs (blue dots) and for the five P2X MEAs (green squares), with the error bars corresponding to the standard deviation for each MEA type. The data were acquired during prolonged load cycling test (switched every 10 min between 0.1 A cm^{-2}, 1.75 A cm^{-2} and 2.0 A cm^{-2}) at 60 °C anode water inlet temperature and ambient pressure.

catalyst, in such a way, that a minimum-maximum corridor for the extrapolation from 3700 h onwards is set). These extrapolated values including the propagated uncertainties would give a mass activity ratio of about 1.4 ± 0.1 at 40,000 h. While this is somewhat less than the ratio of 2.1 that we estimated as the final ratio by our XPS-based analysis of the iridium film thickness ratio (Section 3.1), it is nevertheless reasonably close considering that the estimate involves an extrapolation over an order of magnitude in time.

Assuming that this projection of the time dependence of the OER mass activity is valid, one can then estimate the kinetic voltage loss that is solely due to the OER mass activity loss. For this, we assume that the OER kinetics are described by simple Tafel kinetics (as suggested by Fig. 5), that the overpotential for the HER is negligible,[6] and that the ohmic losses due to membrane and contact resistances are properly accounted for by the HFR. In this case, the iR-free cell voltage ($E_{\mathrm{iR-free}}$) in the absence of other mass-transport related losses can be described by the following equation that is a modification of the equation that was derived by Neyerlin et al. for the iR-free cell voltage in PEM fuel cells (see equation (11) in reference[56]):

$$E_{\mathrm{iR-free}} = 1.5\ \mathrm{V} + \frac{2.303 \cdot R \cdot T}{\alpha_a \cdot F} \cdot \log\left(\frac{i + i_x}{L_{\mathrm{Ir,el}} \cdot i_m^{*(1.5\mathrm{V})} \cdot 10^{-3} \cdot f(p_{O_2}, p_{H_2}) \cdot f(T)}\right) \quad [3]$$

Here, 1.5 V represents the iR-free cell voltage at which the OER mass activity ($i_m^{*(1.5\mathrm{V})}$, in units of A/g$_{Ir}$) is specified, α_a denotes the anodic transfer coefficient, and the prefactor $\frac{2.303 \cdot R \cdot T}{\alpha_a \cdot F}$ before the logarithm term is the Tafel slope TS in (mV/dec). Within the logarithm, i denotes the current density and i_x the current density lost by gas crossover (both in units of A cm^{-2}), $L_{\mathrm{Ir,el}}$ is the OER catalyst loading (in units of mg$_{Ir}$ cm^{-2}), 10^{-3} is a unit conversion factor, and the last two factors, $f(p_{O_2}, p_{H_2})$ and $f(T)$, are gas partial pressure and cell temperature dependent terms (for details, see Eq. 11 in reference[56]). Based on the projected loss in OER mass activity between end-of-test (3700 h) and 40,000 h (see Fig. 7 and above discussion), one can use Eq. 3 to project the kinetic voltage loss that is solely due to the OER mass activity loss, assuming that the Tafel slope does not change significantly over that time (a reasonable assumption based on the negligible change of the Tafel slope between 890 and 3700 h, see Fig. 5), thus using the Tafel slope values determined at 3700 h (given in Fig. 5) as an estimate:

$$\Delta E_{\mathrm{iR-free\ (3700\ h\ \longrightarrow\ 40{,}000\ h)}} = TS_{3700\ \mathrm{h}} \cdot log\left(\frac{i_{m\ (3700\ \mathrm{h})}^{*(1.5\mathrm{V})}}{i_{m\ (40{,}000\ \mathrm{h})}^{*(1.5\mathrm{V})}}\right) \quad [4]$$

Inserting the above extrapolated mass activity values into Eq. (4), the iR-free voltage of the Benchmark catalyst MEAs would be projected to increase by 9 mV between 3700 and 40,000 h, equating to a projected average degradation rate of ≈+0.25 μV/h between 3700 and 40,000 h. In contrast, an increase of 35 mV between 3700 and 40,000 h (or ≈+1.0 μV/h) would be projected for the P2X catalyst. An interesting corollary of Eq. 4 can be drawn for the case when the performance loss of a PEMWE is governed by a loss in OER mass activity that follows the behavior shown here (i.e., $\log(i_m^{*(1.5\mathrm{V})}) \propto log(t)$), the expected loss in iR-free cell voltage of the PEMWE would be proportional to the logarithm of time (i.e., $E_{\mathrm{iR-free}} \propto log(t)$).

For the projected degradation rates (albeit with a high degree of uncertainty), the new P2X catalyst seems to be a promising approach to significantly lower the iridium-specific power density over time scales that are relevant for industrial electrolysis applications. There is, however, a note of caution with regards to the above lifetime extrapolation for the IrO_2/TiO_2 core-shell type catalysts used here. This has to do with the fact that a loss of iridium by dissolution would not be expected to affect the OER mass activity of the catalysts until the IrO_2 shell would be depleted to an extent that the IrO_2 coverage of the TiO_2 core would become incomplete. At that point, the OER mass activity decrease would be expected to accelerate, which we did not observe during our 3700 h test. For the Benchmark catalyst, the thickness of the IrO_2 shell was estimated to ≈10 monolayers,[38] so that one might expect this effect to become visible after an iridium loss of on the order of ≈80% (assuming that an average of two monolayers would still form a complete shell); for the P2X catalyst with an IrO_2 shell thickness of ≈5 monolayers based on our XPS analysis, this effect might become visible after an iridium loss of on the order of ≈60%. Unfortunately, we did not perform any measurements to determine whether there might be a significant loss of iridium from the anode electrode, which would limit the validity of our lifetime estimation of the catalyst. For follow-up studies, we therefore will use extended diagnostic methods to quantify a possible loss of iridium from the anodes during operation.

Finally, we should mention again that this zero-order estimate of the long-term catalyst-specific degradation rates cannot be used for a complete MEA or even cell/stack lifetime estimation, as several other degradation mechanisms may occur (ionomer, membrane, interfacial contact resistances, etc.), which we did not investigate in this study.

Analysis of the HFR decrease over time.—Finally, we want to take a closer look at the decrease of the HFR that is observed over the course of the short stack durability test. Figure 8 shows the averaged HFR values acquired at 0.2 A cm^{-2} of the five individual cells during the complete 3700 h test period for both the Benchmark (blue dots) and the P2X MEAs (green squares). Both MEA types show a similar behavior: After a rather fast decrease of the HFR from its initial value of ≈185 mΩ cm^2 to ≈165 mΩ cm^2 after 500 h, the HFR continues to decrease more gradually until the EOT after 3700 h. At EOT, the average HFR of the Benchmark catalyst MEAs has decreased by ≈52 mΩ cm^2 compared to BOL, which is slightly more than the decrease of ≈39 mΩ cm^2 observed for the P2X MEAs; however, considering the rather large standard deviation of

the HFR for each MEA type, this difference is likely not significant. The overall mean HFR at EOT for all 10 cells is ≈140 mΩ cm^2, corresponding to a ≈45 mΩ cm^2 or ≈25% decrease compared to BOL.

In general, a gradual decrease of the HFR during extended PEMWE has been observed by other researchers[44,52,57]. In principle, the decrease of the HFR over time can have three different reasons, namely: (i) a gradual increase of the water content of the membrane over time,[58,59] which increases the intrinsic conductivity of the ionomer[60]; (ii) a gradual intrusion of the membrane into the pores of the PTL, which decreases the effective membrane thickness[61,62]; and, (iii) a thinning of the membrane due to ionomer chemical degradation.[52,63,64] In this context, we want to note that also membrane degradation can limit the PEMWE MEA lifetime. Typically, a 10% loss in fluoride inventory is considered a failure criterion for Nafion® membranes.[65] As the aim of our study was to conduct a comparison of the durability of the Benchmark and the P2X catalyst, a detailed analysis of the HFR decrease over time was not in our focus. Post-mortem SEM cross-sectional analysis suggested a minor thinning of the membranes over the course of the durability test (on the order of ≈10%), but there was no indication of any loss of mechanical integrity of the membrane that could possibly affect the OER mass activity data.

Conclusions

To validate the durability of a novel low-iridium OER catalyst, we cycled five MEAs with the new low-iridium-loading catalyst at 0.25 mg$_{Ir}$ cm^{-2} and another five MEAs with a Benchmark OER catalyst at 2 mg$_{Ir}$ cm^{-2} together in a 10-cell industrial short stack from H-TEC Systems between 0.1 A cm^{-2}, 1.75 A cm^{-2} and 2.0 A cm^{-2} for 10 min each during 3700 h. Polarization curves and impedance spectra were recorded weekly for every cell in the stack, which allowed for a thorough Tafel-analysis at low current densities and evaluation of the mass-activities of the two different OER catalysts as a function of time over the course of the test campaign. The new catalyst with a significantly lowered iridium packing density shows a 30-fold higher BOL mass-activity at 1.5 V iR-free cell voltage compared to the Benchmark catalyst. Both types of MEAs show an initially faster increase in iR-free cell voltage during the first ≈1000 h which is significantly less pronounced for the rest of the test. The mass activity ratio between the low-iridium loaded catalyst and the Benchmark catalyst decreases during the test and gradually levels out to a value of ≈4 between 1000 and 3700 h. We attribute the rise in iR-free cell voltage visible for both catalyst types (more pronounced for the at beginning-of-life more amorphous novel low-iridium-catalyst and less pronounced for the more crystalline Benchmark catalyst) not to a loss of active material, but to a gradual change in the oxidation state of the surface layer of the catalyst particles from a more active, amorphous hydrous iridium oxide in the beginning to a less active, crystalline IrO_2 during operation. The extrapolated long term degradation rate for the low loading catalyst anodes is higher (≈+1.0 μV/h) than for the benchmark catalyst anodes (≈+0.25 μV/h), but still acceptable low for an industrial application with an additional iR-free cell voltage increase of only ≈35 mV starting from 3700 h onwards to a projected 40,000 h stack lifetime.

Acknowledgments

This work was funded by the German Federal Ministry of Education and Research (BMBF) within the project Kopernikus P2X (funding numbers: 03SFK2I1-2 (ZAE Bayern), 03SFK2V0-2 (Technical University of Munich, Chair of Technical Electrochemistry), 03SFK2R1-2 (H-TEC Systems GmbH), 03SFK2S0-2 (Greenerity GmbH), 03SFK2K1-2 (Heraeus Deutschland GmbH & Co. KG)). The authors gratefully acknowledge Paulette Loichet (Technical University of Munich) and Simon Qian (Technical University of Munich) for valuable discussions and their support on the recording and analysis of the XPS spectra as well as Matthias Rzepka (ZAE Bayern) for valuable discussions.

ORCID

Maximilian Möckl https://orcid.org/0000-0002-1937-9669
Matthias F. Ernst https://orcid.org/0000-0003-2670-3516
Matthias Kornherr https://orcid.org/0000-0002-0201-7506
Hubert A. Gasteiger https://orcid.org/0000-0001-8199-8703

References

1. L. Barreto, A. Makihira, and K. Riahi, "The hydrogen economy in the 21st century: a sustainable development scenario." *International Journal of Hydrogen Energy*, **28**, 267 (2003).
2. M. A. Pellow, C. J. M. Emmott, C. J. Barnhart, and S. M. Benson, "Hydrogen or batteries for grid storage? a net energy analysis." *Energy Environ. Sci.*, **8**, 1938 (2015).
3. B. Emonts, M. Reuß, P. Stenzel, L. Welder, F. Knicker, T. Grube, K. Görner, M. Robinius, and D. Stolten, "Flexible sector coupling with hydrogen: A climate-friendly fuel supply for road transport." *International Journal of Hydrogen Energy*, **44**, 12918 (2019).
4. A. Buttler and H. Spliethoff, "Current status of water electrolysis for energy storage, grid balancing and sector coupling via power-to-gas and power-to-liquids: A review." *Renew. Sustain. Energy Rev.*, **82**, 2440 (2018).
5. T. Bacquart et al., "Hydrogen fuel quality from two main production processes: Steam methane reforming and proton exchange membrane water electrolysis." *Journal of Power Sources*, **444**, 227170 (2019).
6. M. Bernt, A. Siebel, and H. A. Gasteiger, "Analysis of voltage losses in pem water electrolyzers with low platinum group metal loadings." *J. Electrochem. Soc.*, **165**, F305 (2018).
7. M. Carmo, D. L. Fritz, J. Mergel, and D. Stolten, "A comprehensive review on pem water electrolysis." *International Journal of Hydrogen Energy*, **38**, 4901 (2013).
8. K. Ayers, N. Danilovic, R. Ouimet, M. Carmo, B. Pivovar, and M. Bornstein, "Perspectives on low-temperature electrolysis and potential for renewable hydrogen at scale." *Annual Review of Chemical and Biomolecular Engineering*, **10**, 219 (2019).
9. J. Durst, A. Siebel, C. Simon, F. Hasché, J. Herranz, and H. A. Gasteiger, "New insights into the electrochemical hydrogen oxidation and evolution reaction mechanism." *Energy Environ. Sci.*, **7**, 2255 (2014).
10. J. Durst, C. Simon, F. Hasché, and H. A. Gasteiger, "Hydrogen oxidation and evolution reaction kinetics on carbon supported pt, ir, rh, and pd electrocatalysts in acidic media." *J. Electrochem. Soc.*, **162**, F190 (2015).
11. M. Bernt, A. Hartig-Weiss, M. F. Tovini, H. A. El-Sayed, C. Schramm, J. Schröter, C. Gebauer, and H. A. Gasteiger, "Current challenges in catalyst development for pem water electrolyzers." *Chemie Ingenieur Technik*, **92**, 31 (2020).
12. C. K. Mittelsteadt, "PEM electrolysis: Ready for impact." *ECS Trans.*, **69**, 205 (2015).
13. S. Trasatti, "Electrocatalysis by oxides–attempt at a unifying approach." *Journal of Electroanalytical Chemistry and Interfacial Electrochemistry*, **111**, 125 (1980).
14. M. A. Hubert et al., "Acidic oxygen evolution reaction activity–stability relationships in ru-based pyrochlores." *ACS Catal.*, **10**, 12182 (2020).
15. A. Cowley et al., *Pgm Market Report February 2020, Johnson Matthey PLC—Downloaded at 04.02.2022* (2020), https://matthey.com/-/media/files/press-releases/pgm-market-report-february-2020.pdf.
16. F. Price, *The Platinum Standard 2021, Heraeus and SFA Oxford Ltd—Downloaded at 04.02.2022* (2021), https://www.heraeus.com/media/media/hpm/doc_hpm/precious_metal_update/The_Platinum_Standard_2021.pdf.
17. U. Babic, M. Suermann, F. N. Büchi, L. Gubler, and T. J. Schmidt, "Review–identifying critical gaps for polymer electrolyte water electrolysis development." *J. Electrochem. Soc.*, **164**, F387 (2017).
18. M. Bernt, J. Schröter, M. Möckl, and H. A. Gasteiger, "Analysis of gas permeation phenomena in a PEM water electrolyzer operated at high pressure and high current density." *J. Electrochem. Soc.*, **167**, 124502 (2020).
19. S. Siracusano, C. Oldani, M. Assunta Navarra, S. Tonella, L. Mazzapodia, N. Briguglio, and A. Arico, "Chemically stabilised extruded and recast short side chain aquivion proton exchange membranes for high current density operation in water electrolysis." *Journal of Membrane Science*, **578**, 136 (2019).
20. M. Bernt and H. A. Gasteiger, "Influence of ionomer content in iro2/tio2 electrodes on pem water electrolyzer performance." *J. Electrochem. Soc.*, **163**, F3179 (2016).
21. M. Möckl, M. Bernt, J. Schröter, and A. Jossen, "Proton exchange membrane water electrolysis at high current densities: Investigation of thermal limitations." *International Journal of Hydrogen Energy*, **45**, 1417 (2020).
22. M. Schalenbach, M. Carmo, D. L. Fritz, J. Mergel, and D. Stolten, "Pressurized pem water electrolysis: Efficiency and gas crossover." *International Journal of Hydrogen Energy*, **38**, 14921 (2013).
23. P. Trinke, B. Bensmann, and R. Hanke-Rauschenbach, "Current density effect on hydrogen permeation in pem water electrolyzers." *International Journal of Hydrogen Energy*, **42**, 14355 (2017).
24. C. Klose, P. Trinke, T. Böhm, B. Bensmann, S. Vierrath, R. Hanke-Rauschenbach, and S. Thiele, "Membrane interlayer with pt recombination particles for reduction of the anodic hydrogen content in PEM water electrolysis." *J. Electrochem. Soc.*, **165**, F1271 (2018).

25. S. Garbe, U. Babic, E. Nilsson, T. J. Schmidt, and L. Gubler, "Communication-pt-doped thin membranes for gas crossover suppression in polymer electrolyte water electrolysis." *J. Electrochem. Soc.*, **166**, F873 (2019).
26. F. Pantò, S. Siracusano, N. Briguglio, and A. S. Aricò, "Durability of a recombination catalyst-based membrane-electrode assembly for electrolysis operation at high current density." *Applied Energy*, **279**, 115809 (2020).
27. A. Stähler, M. Stähler, F. Scheepers, W. Lehnert, and M. Carmo, "Scalable implementation of recombination catalyst layers to mitigate gas crossover in PEM water electrolyzers." *J. Electrochem. Soc.*, **169**, 034522 (2022).
28. S. Grigoriev, P. Millet, S. Korobtsev, V. Porembskiy, M. Pepic, C. Etievant, C. Puyenchet, and V. Fateev, "Hydrogen safety aspects related to high-pressure polymer electrolyte membrane water electrolysis." *International Journal of Hydrogen Energy*, **34**, 5986 (2009).
29. P. Mazúr, J. Polonský, M. Paidar, and K. Bouzek, "Non-conductive tio2 as the anode catalyst support for pem water electrolysis." *International Journal of Hydrogen Energy*, **37**, 12081 (2012).
30. V. K. Puthiyapura, M. Mamlouk, S. Pasupathi, B. G. Pollet, and K. Scott, "Physical and electrochemical evaluation of ato supported iro2 catalyst for proton exchange membrane water electrolyser." *Journal of Power Sources*, **269**, 451 (2014).
31. D. Böhm, M. Beetz, M. Schuster, K. Peters, A. G. Hufnagel, M. Döblinger, B. Böller, T. Bein, and D. Fattakhova-Rohlfing, "Efficient oer catalyst with low ir volume density obtained by homogeneous deposition of iridium oxide nanoparticles on macroporous antimony-doped tin oxide support." *Adv. Funct. Mater.*, **30**, 1906670 (2020).
32. C. Hao, H. Lv, C. Mi, Y. Song, and J. Ma, "Investigation of mesoporous niobium-doped tio2 as an oxygen evolution catalyst support in an spe water electrolyzer." *ACS Sustainable Chemistry & Engineering*, **4**, 746 (2016).
33. A. G. Hufnagel, S. Häringer, M. Beetz, B. Böller, D. Fattakhova-Rohlfing, and T. Bein, "Carbon-templated conductive oxide supports for oxygen evolution catalysis." *Nanoscale*, **11**, 14285 (2019).
34. H. Xu, B. Rasimick, R. Stone, S. Zhao, and L. Yan, "High-performance, long-lifetime catalysts for proton exchange membrane electrolysis." *Annual Progress Report, Giner Inc.*, **II.B.2**, 1 (2017), https://www.hydrogen.energy.gov/pdfs/progress17/ii_b_2_xu_2017.pdf.
35. T. Hrbek, P. Kúš, Y. Yakovlev, J. Nováková, Y. Lobko, I. Khalakhan, V. Matolín, and I. Matolínová, "Sputter-etching treatment of proton-exchange membranes: Completely dry thin-film approach to low-loading catalyst-coated membranes for water electrolysis." *International Journal of Hydrogen Energy*, **45**, 20776 (2020).
36. K. Lewinski, D. van der Vliet, and S. Luopa, "Nstf advances for pem electrolysis." *ECS Trans.*, **69**, 893 (2015).
37. Kopernikus p2x project funded by the german ministry of education and research, (BMBF) - accessed at 16.02.2022 (2022). https://www.kopernikus-projekte.de/projekte/p2x.
38. M. F. Tovini, A. M. Damjanovic, H. A. El-Sayed, J. Speder, C. Eickes, J.-P. Suchsland, A. Ghielmi, and H. A. Gasteiger, "Degradation mechanism of an IrO2 anode co-catalyst for cell voltage reversal mitigation under transient operation conditions of a PEM fuel cell." *J. Electrochem. Soc.*, **168**, 064521 (2021).
39. M. Bernt, C. Schramm, J. Schröter, C. Gebauer, J. Byrknes, C. Eickes, and H. A. Gasteiger, "Effect of the irox conductivity on the anode electrode / porous transport layer interfacial resistance in pem water electrolyzers." *J. Electrochem. Soc.*, **168**, 084513 (2021).
40. T. Reier, D. Teschner, T. Lunkenbein, A. Bergmann, S. Selve, R. Kraehnert, R. Schlögl, and P. Strasser, "Electrocatalytic oxygen evolution on iridium oxide: Uncovering catalyst-substrate interactions and active iridium oxide species." *J. Electrochem. Soc.*, **161**, F876 (2014).
41. S. Geiger, O. Kasian, B. R. Shrestha, A. M. Mingers, K. J. J. Mayrhofer, and S. Cherevko, "Activity and stability of electrochemically and thermally treated iridium for the oxygen evolution reaction." *J. Electrochem. Soc.*, **163**, F3132 (2016).
42. D. Böhm, M. Beetz, C. Gebauer, M. Bernt, J. Schröter, M. Kornherr, F. Zoller, T. Bein, and D. Fattakhova-Rohlfing, "Highly conductive titania supported iridium oxide nanoparticles with low overall iridium density as oer catalyst for large-scale pem electrolysis." *Applied Materials Today*, **24**, 101134 (2021).
43. K. Ayers, N. Danilovic, K. Harrison, and H. Xu, "Pem electrolysis, a forerunner for clean hydrogen." *The Electrochemical Society Interface*, **30**, 67 (2021).
44. C. Rakousky, U. Reimer, K. Wippermann, M. Carmo, W. Lueke, and D. Stolten, "An analysis of degradation phenomena in polymer electrolyte membrane water electrolysis." *Journal of Power Sources*, **326**, 120 (2016).
45. J. Knöppel, M. Möckl, D. Escalera-Lopez, K. Stojanovski, M. Bierling, T. Böhm, S. Thiele, R. Matthias, and S. Cherevko, "On the limitations in assessing stability of oxygen evolution catalysts using aqueous model electrochemical cells." *Nat. Commun.*, **12**, 2231 (2021).
46. T. Okada, "Effect of ionic contaminants." *Handbook of Fuel Cells*, **3**, 627 (2003).
47. N. Li, S. S. Araya, X. Cui, and S. K. Kær, "The effects of cationic impurities on the performance of proton exchange membrane water electrolyzer." *Journal of Power Sources*, **473**, 228617 (2020).
48. A. Weiß, A. Siebel, M. Bernt, T.-H. Shen, V. Tileli, and H. A. Gasteiger, "Impact of intermittent operation on lifetime and performance of a PEM water electrolyzer." *J. Electrochem. Soc.*, **166**, F487 (2019).
49. M. P. Seah and W. A. Dench, "Quantitative electron spectroscopy of surfaces: A standard data base for electron inelastic mean free paths in solids." *Surface and Interface Analysis*, **1**, 2 (1979).
50. P. J. Cumpson, "The thickogram: a method for easy film thickness measurement in XPS." *Surface and Interface Analysis*, **29**, 403 (2000).
51. J. H. Scofield, "Hartree-slater subshell photoionization cross-sections at 1254 and 1487 ev." *J. Electron Spectrosc. Relat. Phenom.*, **8**, 129 (1976).
52. S. Siracusano, S. Trocino, N. Briguglio, F. Pantò, and A. S. Aricò, "Analysis of performance degradation during steady-state and load-thermal cycles of proton exchange membrane water electrolysis cells." *Journal of Power Sources*, **468**, 228390 (2020).
53. N. Danilovic, K. E. Ayers, C. Capuano, J. N. Renner, L. Wiles, and M. Pertoso, *plenary) challenges in going from laboratory to megawatt scale PEM electrolysis, ECS Transactions*, **75**, 395 (2016).
54. H. G. Sanchez-Casalongue, M. L. Ng, S. Kaya, D. Friebel, H. Ogasawara, and A. Nilsson, "In-situ observation of surface species on iridium oxide nanoparticles during the oxygen evolution reaction." *Angew. Chem. Int. Ed.*, **53**, 7169 (2014).
55. M. Fujita, I. Arima, H. Goto, S. Konaka, and T. Tada, "The relationship between activity and durability of surface area and catalyst loading of IrOx anode catalyst in proton exchange membrane water electrolysis (PEMWE), ECS Meeting Abstracts MA2020-02."2466 (2020).
56. K. C. Neyerlin, W. Gu, J. Jorne, and H. A. Gasteiger, "Determination of catalyst unique parameters for the oxygen reduction reaction in a PEMFC." *J. Electrochem. Soc.*, **153**, A1955 (2006).
57. S. Siracusano, N. Van Dijk, R. Backhouse, L. Merlo, V. Baglio, and A. Aricò, "Degradation issues of pem electrolysis meas." *Renewable Energy*, **123**, 52 (2018).
58. G. Alberti, R. Narducci, and M. Sganappa, "Effects of hydrothermal/thermal treatments on the water-uptake of nafion membranes and relations with changes of conformation, counter-elastic force and tensile modulus of the matrix." *Journal of Power Sources*, **178**, 575 (2008).
59. G. Alberti and R. Narducci, "Evolution of permanent deformations (or memory) in nafion 117 membranes with changes in temperature, relative humidity and time, and its importance in the development of medium temperature pemfcs." *Fuel Cells*, **9**, 410 (2009).
60. T. E. Springer, T. A. Zawodzinski, and S. Gottesfeld, "Polymer electrolyte fuel cell model." *J. Electrochem. Soc.*, **138**, 2334 (1991).
61. T. Schuler, R. D. Bruycker, T. J. Schmidt, and F. N. Büchi, "Polymer electrolyte water electrolysis: Correlating porous transport layer structural properties and performance: Part i. tomographic analysis of morphology and topology." *J. Electrochem. Soc.*, **166**, F270 (2019).
62. T. Schuler, T. J. Schmidt, and F. N. Büchi, "Polymer electrolyte water electrolysis: Correlating performance and porous transport layer structure: Part II. electrochemical performance analysis." *J. Electrochem. Soc.*, **166**, F555 (2019).
63. F. Fouda-Onana, M. Chandesris, V. Médeau, S. Chelghoum, D. Thoby, and N. Guillet, "Investigation on the degradation of meas for pem water electrolysers part i: Effects of testing conditions on mea performances and membrane properties." *International Journal of Hydrogen Energy*, **41**, 16627 (2016).
64. P. Marocco, K. Sundseth, T. Aarhaug, A. Lanzini, M. Santarelli, A. O. Barnett, and M. Thomassen, "Online measurements of fluoride ions in proton exchange membrane water electrolysis through ion chromatography." *Journal of Power Sources*, **483**, 229179 (1919).
65. A. Laconti, H. Liu, C. Mittelsteadt, and R. McDonald, *Polymer electrolyte membrane degradation mechanisms in fuel cells—findings over the past 30 years and comparison with electrolyzers, ECS Transactions*, **1**, 199 (2006).